CHEMISTRY OF MATERIALS

ARTICLE

pubs.acs.org/cm

Counterion Dynamics in Polyurethane-Carboxylate Ionomers with Ionic Liquid Counterions

Shih-Wa Wang,[†] Wenjuan Liu,[‡] and Ralph H. Colby*[,‡]

[†]Department of Chemical Engineering and [‡]Department of Materials Science and Engineering, The Pennsylvania State University, University Park, Pennsylvania 16802, United States

ABSTRACT: Polyurethane carboxylate ionomers based on poly(ethylene glycol) (M_n = 600) with sodium and various ammonium, phosphonium and imidazolium cations are synthesized for systematic comparison of different cationic counterions. Generally, larger cations act as plasticizers, lowering T_g because of weaker Coulombic force for ion associations (acting as physical cross-links). T_g can be reduced from 47 °C to −6 °C when replacing Na^+ with large ether-oxygen containing ammonium without changing polymer composition and the lower T_g can enhance ionic conductivity by 5 orders of magnitude. Ionic conductivity has a stronger correlation with segmental relaxation than T_g, suggesting that counterion motion is coupled to the poly(ethylene oxide) local motions. An electrode polarization model is used to quantify the conducting ion concentration and mobility. All cation mobility follows VFT behavior, whereas conducting ion concentration has an Arrhenius temperature dependence, with slope providing activation energy and intercept determining the fraction of counterions available to participate in ionic conduction. Sodium counterions are mostly trapped by pPDI-carboxylate-pPDI segments, whereas the larger counterions are less trapped. Cation species and methoxyalkyl tails were found to impact both conducting ion concentration and their mobility but T_g and α-relaxation time are the key factors for ionic conductivity at a given temperature.

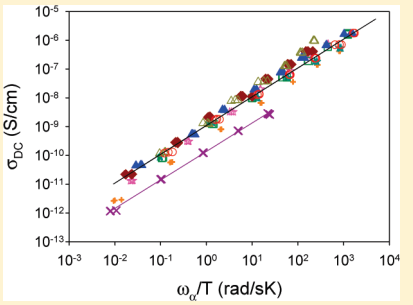

KEYWORDS: ionic conductors, polymeric materials

INTRODUCTION

Many applications of polymer ion conductors simultaneously require high ionic conductivity and high modulus. Lithium ion battery separator membranes and ion-transport actuators are two high-profile examples. Polyethylene glycol (PEG or PEO) and PEO-based polymer electrolytes have been the mainstream research focus since 1973 because of their excellent ability to solvate cations.[1−3] Although PEO-based homopolymer electrolytes have reasonable ionic conductivities, many of them suffer from poor mechanical strength due to the low glass-transition temperature (T_g) of PEO.[4] Ionic conductivity benefits from the fast segmental motion of low T_g materials but the modulus is at best the plateau modulus of the polymer melt (~1×10^6 Pa). With single-phase systems, ionic conductivity increases and modulus decreases as T_g is lowered, resulting in a correlation (trade-off) between modulus and conductivity.[4]

To obtain materials with simultaneous high modulus and high conductivity, polymers that spontaneously microphase separate into hard domains (high modulus) and soft domains that transport ions, are needed. Block copolymers have been used[5,6] but here we focus on segmented copolymers. Polyurethane (PU) ionomers can be quite interesting candidates, as their microphase separation can allow a hard phase that provides high modulus to coexist with a continuous soft phase that transports ions. Various strategies have been used to attach ionic groups to polyurethanes.[7−10] Different metal cations can change T_g and morphology. The modulus can reach 1×10^7 to 1×10^9 Pa even far above the T_g of the soft phase when attaching ionic groups in the hard segment.[11−13] In terms of ionic conductivity, 1×10^{-7} to 1×10^{-8} S/cm at room temperature has been achieved for Li^+ or Na^+ counterions, with modulus of 1×10^8 Pa when replacing the urethane proton with a sulfonated group in the hard segment.[14]

However, unlike the many studies of mechanical properties of PU ionomers,[7,8] conductivity and dielectric studies are less common and more focusing on varying metal counterions.[15] Dielectric relaxation spectroscopy (DRS) has proved to be a very useful tool for PU ionomer studies.[16,17] Combined with thermal and mechanical tests, DRS allows understanding of both microphase separation and dipole/polymer chain relaxation in the soft phase, as well as ionic conductivity.[17−19]

In this paper, PEG with M_n = 600 and M_w/M_n < 1.2 was chosen as the soft segment because of its famous ability to solvate cations[1−3] and being short enough to inhibit crystallization. About 2 orders of magnitude higher ionic conductivity has been reported for PEO- than poly(tetramethylene oxide)-based PU ionomers.[18,20] Para-Phenylene diisocyanate (pPDI) was used as the hard segment because its symmetry facilitates microphase separation.[21,22] Carboxylic acid containing diol was used as the chain extender, effectively placing the ionic group between two pPDI segments. By varying from the small alkali metal Na^+ to

Received: December 13, 2010
Revised: January 18, 2011
Published: March 01, 2011

large multiatom cations like ammonium, imidazolium and phosphonium, we hope to understand how both the counterion size and species affect the morphology, T_g, conductivity, dielectric constant, conducting ion content and mobility in PU ionomers, with particular consideration of their utility for ionic actuators. A principal finding is that these materials do not microphase separate in the conventional sense but counterions are trapped by the pPDI-carboxylate-pPDI segments, unable to participate in ionic conduction.

MATERIALS

Para-phenylene diisocyanate (pPDI), 2,2-bis(hydromethyl)butyric acid (DMBA), sodium hydroxide, 4-methylmorpholine, iodomethane, tris[2−2(-methoxyethoxy)ethyl]amine, tetrabutylammonium hydroxide-30 hydrate (Bu_4N^+-OH), tributyl phosphine, tetrabutylphosphonium hydroxide (40 wt % aqueous solution) (Bu_4P^+-OH), N-methylimidazole and butyl-methyl-imidazolium chloride ($BuMeIm^+$-Cl) were purchased from Aldich. Tetramethylammonium hydroxide-5 hydrate (Me_4N^+-OH) was purchased from Fluka. Polyethylene glycol (PEG, M_n = 600 and M_w/M_n < 1.2 from the manufacturer and confirmed by aqueous SEC and ^{1}H NMR in DMSO-d_6) and 2-bromoethyl methyl ether were purchased from TCI America, Inc. Anhydrous N,N-dimethylformamide (DMF) and diethyl ether were purchased from EMD. Anionic ion-exchange resin Amberlite IRA-400 was purchased from Alfa Aesar. pPDI was purified by sublimation at 80 °C under vacuum as in literature.[21] PEG 600 was vacuum-dried at 80 °C for at least 24 h before use. All other chemicals were used as received.

Carboxylic Acid Containing Polyurethane (PU) Synthesis. pPDI, PEG 600 and DMBA with the molar ratio of 2:1:1 were dissolved in anhydrous DMF and reacted at 60 °C. The chemical structure of the product polyurethane is shown in Scheme 1. It is a random segmented copolymer with pPDI segments between PEG 600 and carboxylic acid sections. The reaction was monitored by FTIR until the isocyanate peak (~2200 cm^{-1}) disappears (in 4−5 h). Synthesized products were precipitated in diethyl ether 3 times and dried at 80 °C under vacuum. The final purification was done by dialysis after neutralization to make the carboxylate ionomers, which are water-soluble.

Counterion Synthesis. *Tris[2−2(methoxyethoxy)ethyl]methyl Ammonium Iodide ($(MOEOE)_3MeN^+$-I).* Tris[2−2(methoxyethoxy) ethyl]amine and 50% excess of iodomethane were dissolved in toluene and charged into a round-bottom flask in an ice bath. The mixture was allowed to reach room temperature and react overnight. The product was a dark yellow liquid that phase separated from the raw material and was purified by extraction with toluene then dried at 70 °C under vacuum. ^{1}H NMR (D_2O): δ 3.17 (s, 3H, -N^+-CH_3); 3.33 (s, 9H, -O-CH_3); 3.58, 3.59 (d, 12H, -O-CH_2CH_2-O-); 3.69 (s, 6H, N^+-CH_2-CH_2-O-); 3.91 (s, 6H, -N^+-CH_2-CH_2-O-).

N-(2-methoxyethyl)-N-methylmorpholinium Bromide ($(EOc)_2Me(MOE)N^+$-Br). 2-Bromoethyl methyl ether and 100% excess N-methylmorpholinium were reacted at 70 °C overnight. The product was dissolved in methanol and recrystallized in an excess of acetone. The white crystal product was then dried at 70 °C under vacuum. ^{1}H NMR (D_2O): δ 3.19 (s, 3H, -N^+-CH_3); 3.31 (s, 3H, -O-CH_3); 3.4−3.5 (m, 4H, -N^+-CH_2-CH_2-O-); 3.97 (s, 4H, -N^+-CH_2-CH_2-O-); 3.66 (s, 2H, -N^+-CH_2-CH_2-O-CH_3); 3.85 (s, 2H, -N^+-CH_2-CH_2-O-CH_3).

(2-Methoxyethyl)-tributylphosphonium Bromide ($Bu_3(MOE)P^+$-Br). Tributyl phosphine and 2-bromoethyl methyl ether with 10% excess were reacted at 80 °C for 1 day. The product was washed with a large amount of diethyl ether 3 times and vacuum-dried at 70 °C. ^{1}H NMR (DMSO-d_6): δ 0.92 (t, 9H, -CH_3); 1.3−1.5 (m, 12H, -P^+-CH_2-CH_2-CH_2-CH_3); 2.2 (t, 6H, -P^+-CH_2-CH_2-CH_2-CH_3); 2.6 (m, 2H, -P^+-CH_2-CH_2-O-); 3.3 (s, 3H, -O-CH_3); 3.6 (m, 2H, -CH_2-O−).

Methoxyethyl Methyl Imidazolium Bromide ($(MOE)MeIm^+$-Br). N-methylimidazole and 20% excess 2-bromoethyl methyl ether were reacted at 40 °C for 1 day. The product was washed and recrystallized in diethyl ether and dried at 70 °C under vacuum. ^{1}H NMR (DMSO-d_6): 3.27 (s, 3H, -N-CH_3); 3.68 (t, 2H, -N-CH_2-CH_2-O-); 3.88 (s, 3H, -O-CH_3); 4.36 (t, 2H, -N-CH_2-CH_2-O-); 7.7 (d, 2H, -N-CH=CH-N-); 9.16 (t, 1H, -N-CH-N-).

Ion exchange, Purification, and Molecular Weight. The ammonium and phosphonium salts above were ion exchanged with Amberlite IRA-400 ion-exchange resin to prepare hydroxide aqueous solutions and stored in a refrigerator for later use. The concentration was determined by titration with 0.1N HCl standard solution.

One gram of the carboxylic acid containing polyurethane was dissolved in the counterion- hydroxide aqueous solution (with 10% excess hydroxide to ensure 100% neutralization) and then dialyzed in a dialysis cassette (MW cutoff = 2000) in deionized water for 1 week to remove any extra ions. The product was then dried at 70 °C under vacuum. The dried PU ionomers are fully water-soluble. The ionomer with counterion structures and some physical properties are summarized in Scheme 1 and Table 1. The Ionomer has M_w = 12000, M_n = 8400, M_w/M_n = 1.4 (polystyrene equivalent molar masses) determined by size exclusion chromatography with 0.01 M LiBr DMF solution as the mobile phase. This number agrees with the estimation (M_n = 9000) by ^{1}H NMR. The cation to ether oxygen ratio is 1/13.

***Ab initio* Calculation.** In this study, *ab initio* calculations were employed to determine interaction energies of quadrupoles (Table 1), and the charge distribution of cations (Table 2). All calculations were

Scheme 1. Chemical Structures of Polyurethane Anionomer and Cations Studied: Na^+, Me_4N^+, Bu_4N^+, $(EOc)_2Me(MOE)N^+$, $(MOEOE)_3MeN^+$, $BuMeIm^+$, $(MOE)MeIm^+$, Bu_4P^+, $Bu_3(MOE)P^+$ (from left to right, top to bottom)

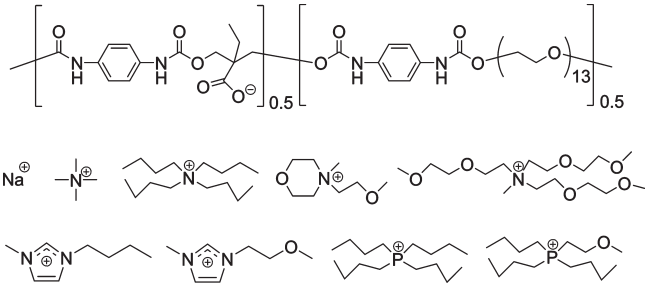

Table 1. Cation−Anion Distance,[a] Glass Transition Temperature and Quadrupole Formation Energy $\Delta E_{quadrupole}$[b] of the Ion Pair Calculated by *ab initio* at 0K in Vacuum

	$[M/(\rho N_{av})]^{1/3}$ (Å)	T_g (K)	$\Delta E_{quadrupole}$ (kJ/mol)
Na^+	5.1	323	1400
Me_4N^+	6.0	308	930
$BuMeIm^+$	6.9	304	880
$(MOE)MeIm^+$	6.9	298	890
$(EO_c)_2Me(MOE)N^+$	7.0	291	860
Bu_4N^+	7.9	289	820
Bu_4P^+	8.1	273	790
$Bu_3(MOE)P^+$	8.1	284	790
$(MOEOE)_3MeN^+$	8.7	267	900

[a] Cation-anion distance is calculated from the molar mass of the cation-acetate salt, assuming density ρ = 1 g/cm^3. [b] $\Delta E_{quadrupole}$ is defined as the energy difference between the quadrupole state and 2 free cations plus 2 free anions at 0 K in vacuum.

dx.doi.org/10.1021/cm103548t |*Chem. Mater.* 2011, 23, 1862–1873

Table 2. Charge Distribution of Bu_4P^+, Bu_4N^+ and BuMeIm$^+$ from *ab initio* Calculation

	center (P or N)	α-CH_2	β-CH_2	CH_3	CH=CH	CH
Bu_4P^+	1.1	−0.2	0			
Bu_4N^+	−0.5	0.3	0			
BuMeIm$^+$	−0.3, −0.3	0.4	0	0.4	0.2	0.4

performed using density functional theory methods with the Gaussian 03 software package. Exchange and correlation were included using the hybrid-GGA B3LYP functional.[23−26] Dipole moments of polar solvents and energy of interactions of polar solvents with ions agree with vapor phase data[27] for the basis set used.

Differential Scanning Calorimetry (DSC). The calorimetric glass transition temperature T_g was measured using a Seiko Instruments SSC/5200 (Table 1). All samples were dried at 75 °C under vacuum for 2 days before measurement. T_g was obtained from the change in heat capacity during the second heating at a heating rate of 10 K/min under dry nitrogen purge after cooling from 80 °C at 10 K/min.

Rheology. Linear viscoelastic response was probed in oscillatory shear using a Rheometrics RDS-II. All samples were dried at 75 °C under vacuum for 2 days and then molded to ∼1 mm thick pellets with diameter of either 4 mm (for Na^+, Me_4N^+, BuMeIm$^+$, and (MOE)-MeIm$^+$) or 7.9 mm (for all other samples) at 80 °C under vacuum for 20 min. The temperature step data were collected every 1 °C from 30 to 80 °C at 1 rad/s with 60 s soak time.

Dielectric Relaxation Spectroscopy (DRS). Samples were dried at 75 °C under vacuum for 1 day to remove moisture and then sandwiched between two 20 mm diameter freshly polished brass electrodes with 50−100 μm silica fiber spacers. The prepared cells were annealed in the vacuum oven for an additional 24 h at 75 °C under vacuum. Dielectric (impedance) spectra were measured using a Novocontrol GmbH Concept 40 broadband dielectric spectrometer in the frequency range of 1×10^{-2} to 1×10^{7} Hz with 0.1 V amplitude. Samples were annealed at 80 °C in the equipment for 1 h and then allowed to reach equilibrium with temperature for at least 30 min before each isothermal measurement.

RESULTS AND DISCUSSIONS

Glass Transition Temperature (T_g). As described in the literature, different metal cations can have very different impact on T_g, depending on the chemical composition of the PU ionomers.[11,28] In our system, only one T_g has been seen and T_g decreases dramatically with increasing cation size. Figure 1(a) shows T_g as a function of inverse size of corresponding cation-acetate salts (assuming all the salts have the same density of 1 g/cm^3). The precursor acid form PU has T_g = 23 °C. Introduction of small sodium ions increases the T_g to 47 °C. The increase of T_g with alkali metal counterions is common,[29] possibly originating from some combination of (1) mixing soft and hard segment and (2) the Coulombic force between cations and anions acting as physical cross-links. The PEO soft segment is well-known for its ability to solvate cations so it is not surprising that the presence of sodium cations in the hard segment helps mix the soft and hard segment, increasing the T_g. Simultaneously, with Na^+ counterions, many ion pairs associate, which also increases T_g. Other evidence of phase mixing in the Na-ionomer is that it has much higher T_g than a PEG600 based polyester ionomer PEG600-Na^+ (T_g = −5 °C) with similar ion concentration.[30] Although nonionic PU with pPDI hard segment tends to microphase separate,[21] there is no

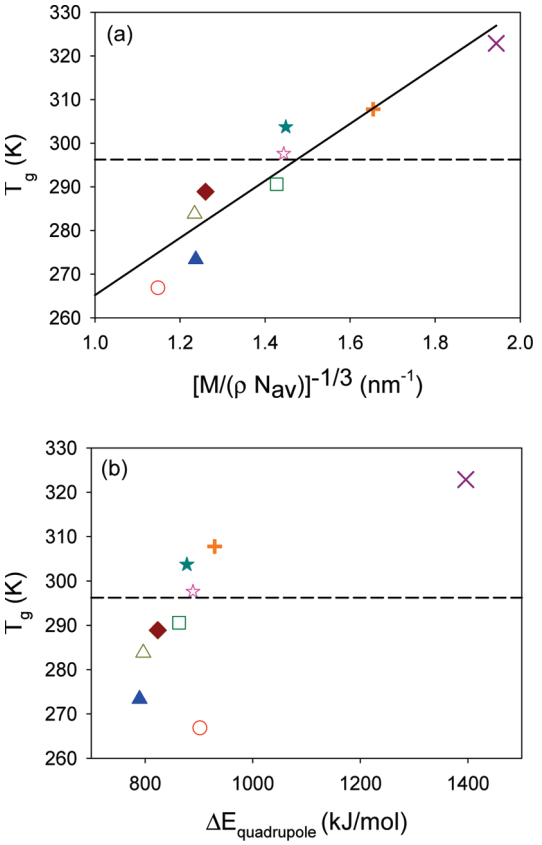

Figure 1. T_g from DSC as a function of (a) reciprocal size of corresponding acetate salts (assuming the same density ρ of 1.0 g/cm^3) and (b) quadrupole energy at 0K in vacuum. Open symbols are cations containing ether oxygen. Solid symbols are cations without ether oxygen. Purple X is Na^+; orange plus is Me_4N^+; cyan solid star is BuMeIm$^+$; pink open star is (MOE)MeIm$^+$; green open square is $(EOc)_2Me(MOE)N^+$; dark red solid diamond is Bu_4N^+; blue solid triangle is Bu_4P^+; olive green open triangle is $Bu_3(MOE)P^+$; red open circle is $(MOEOE)_3MeN^+$; dash line is acid form for the reference; solid line is fitting result of equation $T_g = 200 + 65.4\,[M/(\rho N_{av})]^{-1/3}$.

evidence from our DSC study for microphase separation in both the acid form precursor and the ionomers.

It is clear in Figure 1a that T_g scales inversely with cation acetate salt size. Similar phenomena with various metal ions have also been observed in different ionomer systems.[28,31,32] Ion pairs associate to form physical cross-links and T_g reflects the energy required to separate associated ion pairs.[31,33] Larger cations have a longer distance between the positive and negative charge and require much less energy to separate them, originating from Coulomb's law: $E \sim e^2/d$, where e and -e are charges carried by cation and anion and d is the distance between two charges. The lower interaction energy results in reduced T_g with an apparent inverse correlation with the ion size. Meanwhile, lower T_g also indicates fewer ionic cross-links[11,12] also due to weaker Coulombic interaction.

T_g as a function of quadrupole energy (energy required to break quadrupoles) from *ab initio* calculation is also plotted in Figure 1b. It shows similar results as Figure 1a since quadrupole energy is strongly affected by counterion size due to Coulombic force. It is interesting that $(MOEOE)_3MeN^+$ has the lowest T_g. The quadrupole energy of $(MOEOE)_3MeN^+$ is not the lowest (an outlier in Figure 1(b)), possibly because

dx.doi.org/10.1021/cm103548t |*Chem. Mater.* 2011, 23, 1862–1873

this energy is calculated at 0K under vacuum without consideration of any entropy contribution, which might be more important for $(MOEOE)_3MeN^+$ due to its three much longer side chains.

Note also that tetrabutylphosphonium (Bu_4P^+) has T_g 20K lower than tetrabutylammonium (Bu_4N^+) despite similar size and chemical structure. This is due to the different electronegativity[34] of the nitrogen and phosphorus atoms in these two cations. Table 2 shows the charge distribution of three classes of cations we study in this paper: Bu_4P^+, Bu_4N^+, and $BuMeIm^+$. The phosphorus atom at the center of Bu_4P^+ carries positive charge (+1.1e) because it is less electronegative than carbon and leaves the outer atoms to share −0.1e, whereas the nitrogen atom in Bu_4N^+ is more electronegative than carbon and carries negative charge (−0.5e) and leaves the surrounding atoms sharing +1.5e. The negatively charged outer layer of Bu_4P^+ provides better shielding of the positive charge at the center from anions, resulting in weaker Coulombic force and lower T_g (the two phosphonium cations have the smallest quadrupole energy in Table 1 for the same reason). For Bu_4N^+, the more positively charged molecule surface has stronger attraction with anions and thus has higher T_g. For imidazolium, although the nitrogen atom still is weakly negative like ammonium, the steric structure is very different. The nearly flat structure of the imidazole ring makes most of the atoms exposed to anions have a shorter effective distance compared to the tetrahedral ammonium and phosphonium, raising T_g of the ionomers with imidazolium counterions relative to the similar sized $(EOc)_2Me(MOE)N^+$ ammonium. It is also interesting that attachment of ether-oxygen containing alkyl chains to the counterions have different effects on T_g: T_g is suppressed in ammonium and imidazolium but raised in phosphonium, again because of the the electronegativity of C, O, N, and P and different charge distributions. Ether-oxygen makes the adjacent carbon more positively charged which changes the surface charge distribution of phosphonium and increases T_g. In ammonium and imidazolium, where carbon atoms already carry positive charges, ether oxygens provide some shielding from anions and decrease T_g.

Rheology and Morphology. Storage and loss modulus G' and G'' and tan δ in temperature sweeps at 1 rad/s as functions of T/T_g are plotted in Figure 2a. As expected, ionomers with larger counterions have smaller G' and G''.[35,36] Only Na^+, Me_4N^+, $BuMeIm^+$, $(MOE)MeIm^+$, $Bu_3(MOE)P^+$ and $(MOEOE)_3MeN^+$ data are shown. Other samples have similar behavior with $Bu_3(MOE)P^+$ and $(MOEOE)_3MeN^+$ and were omitted for clarity. Imidazolium-based ionomers show different character than the other ionomers. $BuMeIm^+$ and $(MOE)MeIm^+$ ionomers both have a clear glass transition peak in tan δ as most homogeneous polymers do, while the $(MOE)MeIm^+$ ionomer also has a small shoulder at higher temperature. On the other hand, Na^+, ammonium and phosphonium ionomers show a glass transition peak at slightly higher T/T_g with a very broad shoulder at higher temperature. The shoulder-like behavior of PU usually indicates microphase separation.[37,38] However, no microphase separation peaks were observed in SAXS measurement for all ionomers (and the acid form precursor; data not shown) while time−temperature superposition works perfectly (Figure 2b) and these both suggest there is no discrete microphase separation. All ionomers collapse into the same curve in a Cole−Cole plot in the Figure 2b **inset**, also suggesting no discrete microphase separation.[39] We believe the broad shoulder in our system is from various local environments[40] (i.e., various concentrations

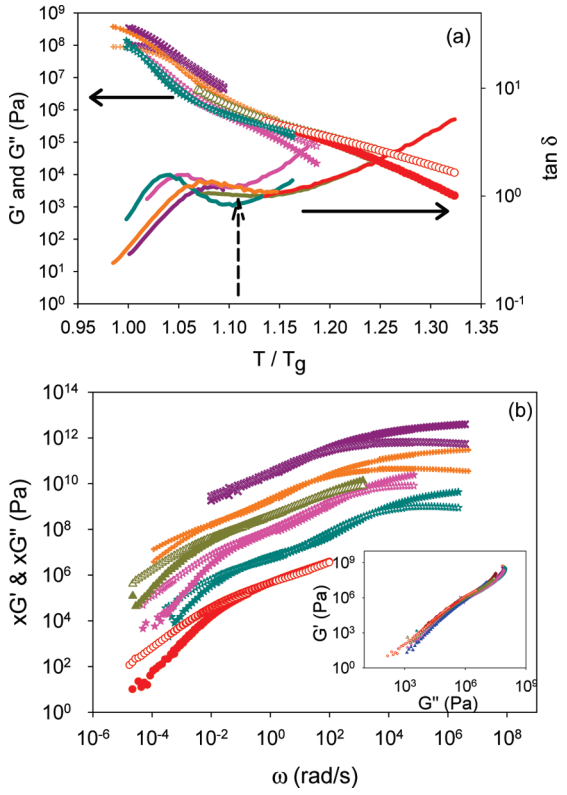

Figure 2. (a) Storage and loss modulus and tan δ (solid curve) as function of T/T_g at 1 rad/s. Dashed arrow indicates the shoulder of nonimidazolium ionomers. (b) Master curves of storage (G', filled symbols) and loss (G'', open symbols) modulus as functions of frequency from time−temperature superposition of oscillatory shear data at various temperatures, shifted to T_g + 30 K. Inset: Cole−Cole plot of oscillatory shear data for all ionomers at various temperatures. Purple X is Na^+ (x = 8000); orange plus is Me_4N^+ (x = 500); cyan star is $BuMeIm^+$ (x = 10); pink star is $(MOE)MeIm^+$ (x = 100); dark red diamond is Bu_4N^+; blue triangle is Bu_4P^+; olive green triangle is $Bu_3(MOE)P^+$ (x = 300); red circle is $(MOEOE)_3MeN^+$ (x = 1); Bu_4N^+, Bu_4P^+ and $(EOc)_2Me(MOE)N^+$ are not shown for clarity.

of pPDI-carboxylate-pPDI/cation segment) resulting in a wide distribution of relaxation times instead of discrete microphase separation. It is also interesting that imidazolium ionomers are more homogeneous than all other ionomers. This is perhaps due to the acidic protons on the ring of imidazolium that are hydrogen bond donors.[41] These can interrupt the hydrogen bonding between urethane linkages more than other counterions as well as have stronger interaction with ether oxygens on PEO segments. Meanwhile, acidity of the protons on the ring can be slightly reduced by having ether oxygen containing tails[41,42] and this perhaps explains why $(MOE)MeIm^+$ has a small shoulder in tan δ compared to $BuMeIm^+$. The local environment differences also impact the amount of counterions available under electric field and we will discuss this later.

Polymer Relaxation. The dielectric loss spectra of ionomers are usually dominated by conduction and electrode polarization (EP) in the low frequency region, which can mask the α-relaxation. Instead of analyzing dielectric loss directly, the common method to remove the pure-loss conductivity contribution is to plot the derivative dielectric loss spectra using the following formula derived from the Kramers−Kronig relation,

dx.doi.org/10.1021/cm103548t |*Chem. Mater.* 2011, 23, 1862–1873

since $\varepsilon'(\omega)$ and $\varepsilon''(\omega)$ must be the real and imaginary parts of the same complex function[16,19,43,44]

$$\varepsilon_{der}(\omega) = -\frac{\pi}{2}\frac{\partial\varepsilon'(\omega)}{\partial \ln \omega} \quad (1)$$

Figure 3 shows the dielectric loss derivative spectra of PU ionomers with different cations, at their T_g. From high to low frequency, the first peak of ε_{der} corresponds to the α (segmental) relaxation, which is revealed by the derivative analysis, and then the rapid increase at lower frequency is EP. ε_{der} and the dielectric loss ε'' are compared in the Figure 3a inset. It is surprising that the α-relaxation at T_g does not occur at the same frequency for larger cations (Bu_4N^+, Bu_4P^+, $Bu_3(MOE)P^+$, and $(MOEOE)_3MeN^+$, which has the lowest T_g) This implies the polymer chain relaxation does not determine the T_g measured with DSC. Instead, T_g is more strongly correlated with the cation−anion interaction (see Figure 1). Besides the α-relaxation peak frequency, the shape of the peak also depends on cation. In Figure 3, only Na^+ (purple X) and Me_4N^+ (orange +) have clear, roughly symmetric peaks, whereas the other cations have asymmetric peaks or merely a shoulder on the high-frequency side of EP.

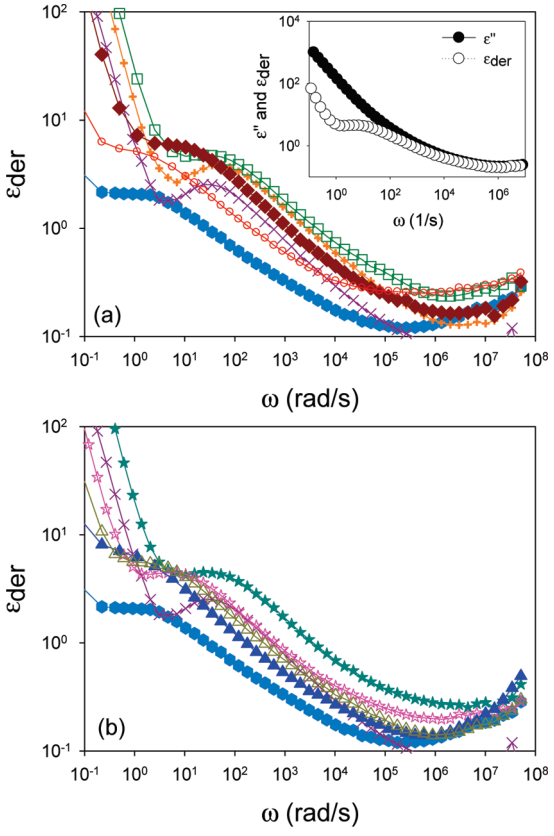

Figure 3. (a) Dielectric loss derivative spectra of Na^+, Me_4N^+, $(EOc)_2Me(MOE)N^+$, Bu_4N^+ and $(MOEOE)_3MeN^+$ ionomers at corresponding $T_g \pm 5$ K. Inset:. Dielectric loss (solid symbol) and derivative (open symbol) spectra of $(MOE)MeIm^+$ at T_g (20 °C). (b) Dielectric loss derivative spectra of Na^+, $BuMeIm^+$, $(MOE)MeIm^+$, Bu_4P^+ and $Bu_3(MOE)P^+$ at corresponding $T_g \pm 5$K. Purple X is Na^+; orange plus is Me_4N^+; cyan solid star is $BuMeIm^+$; pink open star is $(MOE)MeIm^+$; green open square is $(EOc)_2Me(MOE)N^+$; dark red solid diamond is Bu_4N^+; blue solid triangle is Bu_4P^+; olive green open triangle is $Bu_3(MOE)P^+$; red open circle is $(MOEOE)_3MeN^+$; light blue solid hexagon is the acid form (nonionic polymer).

In Figure 3, the α peak height of Na^+ is significantly smaller than others which gives some insight about the local hydrogen bonded pPDI-carboxylate-pPDI segment and soft segments. The magnitude of the α-relaxation in ε_{der} represents the concentration of dipoles that can respond to the electric field.[16,17]

Figure 4 shows the α-relaxation peak frequency, ω_ω as a function of inverse temperature with the inset plotted as a function of T_g/T. ω_α is determined as the frequency where ε_{der} has its peak by fitting the α-peak with the Havriliak−Negami equation[16] after removing the contribution of electrode polarization. The inset of Figure 4 shows that the calorimetric T_g is not directly related to polymer segmental relaxation. It can be seen that the smaller cations show slower α-relaxation due to more and/or stronger association of ion pairs with each other and with urethane linkages. On the other hand, the presence of ether oxygens on the cations accelerates the α-relaxation, except in phosphonium cations.

The temperature dependence of the α-relaxation follows the Vogel−Fulcher−Tammann (VFT) equation (solid curves in Figure 4)

$$\omega_\alpha = \omega_0 \exp\left(-\frac{DT_0}{T - T_0}\right) \quad (2)$$

where ω_0 is the unconstrained (high T) frequency, T_0 is the Vogel temperature, and D is a parameter related to fragility. Table 3 summarizes the VFT fitting parameters for the α-relaxation frequency. There is no correlation between calorimetric T_g and the α-relaxation Vogel temperature T_0. It is worth to note that the data can also be fit using a common $T_0 = 202$ K with $R^2 \geq 0.99$. The Vogel temperature T_0 in our PU ionomer system is similar to other PEG600-based polyester ionomers[43,45] even though our PU ionomers have much higher T_g in DSC. This again confirms that the α-relaxation that we see is corresponding to PEO segmental motion, while the calorimetric T_g is restricted by the cross-link-like ion pair interactions. Nonionic glass-forming liquids and polymers have larger D (lower fragility) associated with stronger intermolecular interactions.[46] Consequently, it is not surprising that D increases as counterions get

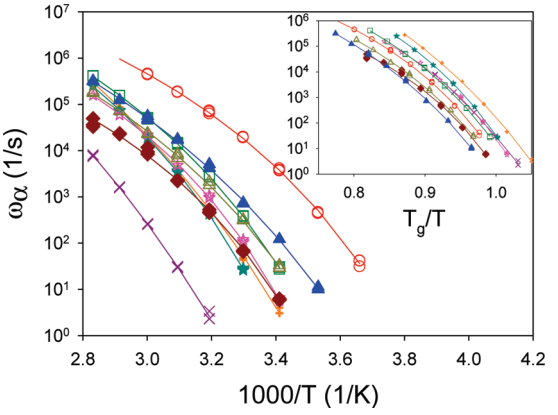

Figure 4. α-Relaxation frequency as a function of temperature. Inset: α relaxation frequency as a function of T_g normalized temperature. Purple X is Na^+; orange plus is Me_4N^+; cyan solid star is $BuMeIm^+$; pink open star is $(MOE)MeIm^+$; green open square is $(EOc)_2Me(MOE)N^+$; dark red solid diamond is Bu_4N^+; blue solid triangle is Bu_4P^+; olive green open triangle is $Bu_3(MOE)P^+$; red open circle is $(MOEOE)_3MeN^+$. Solid line is best fitting for VFT equation (eq 2).

dx.doi.org/10.1021/cm103548t |Chem. Mater. 2011, 23, 1862–1873

Table 3. Fitting Parameters for the Temperature Dependences of α-Relaxation Frequency (eq 2), Conducting Ion Content (eq 10) and Conducting Ion Mobility (eq 11)

		α-relaxation				conducting ion content		conducting ion mobility			
	$[M/(\rho N_{av})]^{1/3}$	T_g	T_0	D	log ω_0	log p_0	E_a (kJ/mol)	T_0	T_g-T_0	D	log μ_0
Na^+	5.1	323	203	16.2	13.5	18*	10*	263	60	3.5	1.9
Me_4N^+	6.0	308	214	9.87	12.1	18.7	5.9	241	67	5.0	0.7
$BuMeIm^+$	6.9	304	228	7.63	11.5	21.1	16	247	57	10.3	3.8
$(MOE)MeIm^+$	6.9	298	233	5.18	9.56	19.5	11	242	56	4.0	1.5
$(EOc)_2Me(MOE)N^+$	7.0	291	225	6.18	10.3	19.5	12	234	56	4.5	0.9
Bu_4N^+	7.9	289	206	9.42	10.5	19.2	11	218	71	7.0	0.2
Bu_4P^+	8.1	273	177	15.8	12.5	19.0	12	205	68	7.7	−0.3
$Bu_3(MOE)P^+$	8.1	284	239	4.73	8.79	18.8	8.8	221	63	6.0	0.3
$(MOEOE)_3MeN^+$	8.7	267	202	7.39	10.7	19.0	7.3	205	62	6.3	0.4

*Uncertainty of the fitting for Na^+ is higher than other samples because of a limited number of data points (50−80 °C).

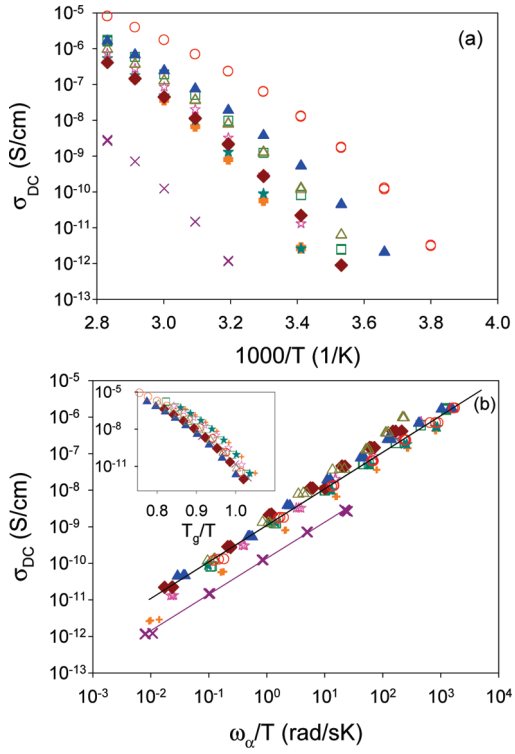

Figure 5. DC conductivity as function of (a) 1000/T, (b) α-relaxation frequency/temperature; inset, T_g/T. Purple X is Na^+; orange plus is Me_4N^+; cyan solid star is $BuMeIm^+$; pink open star is $(MOE)MeIm^+$; green open square is $(EOc)_2Me(MOE)N^+$; dark red solid diamond is Bu_4N^+; blue solid triangle is Bu_4P^+; olive green open triangle is $Bu_3(MOE)P^+$; red open circle is $(MOEOE)_3MeN^+$.

smaller and interact with both carboxylate anion and PEO ether-oxygen more strongly.

Ionic Conductivity. Temperature dependence of DC ionic conductivity (σ_{DC}) is plotted in Figure 5a. It is clear that samples with lower T_g have higher conductivity. At the same time, the presence of ether oxygens on the cations (open symbols in all figures) increases ionic conductivity (compared to cations with only alkyl chains) for ammonium and imidazolium counterions but not for phosphonium counterions (Bu_4P^+ and $Bu_3(MOE)P^+$), which is due to the different effect on T_g discussed above. Figure 5b inset plots DC ionic conductivity against T_g/T, which collapses data compared to Figure 5a but roughly a factor of 40 spread in σ_{DC} remains. It is generally accepted in the literature that ion conduction in PEG-based polymer electrolytes is strongly coupled with polymer chain relaxation.[2,19,43,47] DC conductivity is plotted against α-relaxation frequency in Figure 5b, where data naturally separate into two groups: Na^+ and all other cations. All the ammonium, imidazolium, and phosphonium counterion ionomers have DC ionic conductivity connected to α-relaxation frequency divided by temperature (ω_α/T) as expected by the Debye−Stokes−Einstein equation

$$\frac{\sigma_{DC}}{\omega_\alpha/T} = 1.09 \times 10^{-9} \frac{\text{SsK}}{\text{cm rad}} \quad (3)$$

shown as the upper solid line in Figure 5b. The fact that eq 3 applies to all counterions other than Na^+ suggests they have similar concentrations of conducting counterions. The fact that σ_{DC} is a factor of 6 lower for Na^+ suggests that the pPDI-carboxylate-pPDI segments may trap most of the Na^+ and this will be discussed further when we quantify conducting ion content.

The slope of 1 in Figure 5b means the ion conduction is regulated by PEO segmental motion. Note that all the samples should contain the same amount of ions since they are prepared from the same acid form precursor but the actual amount of the cations that are really accessible in the matrix might be lower and change with temperature. It is interesting that we do not observe decoupling (slope lower than unity in Figure 5b) as observed in our previous study[43] of PEG-based polyester ionomers.

Electrode Polarization (EP) Model. DC conductivity (σ_{DC}) of any single-ion conductor is simply the product of charge, mobility (μ) and number density (p) of ions participating in conduction:

$$\sigma_{DC} = e\mu p \quad (4)$$

where e is the elementary charge (of all monovalent cations). Although all "nontrapped" counterions in the soft phase eventually contribute equally to conduction, our interest here is the number density of conducting ions in a given instant in time, and their mobility. We make use of an electrode polarization (EP) model (Macdonald/Coelho model)[19,30,48,49] that integrates the Poisson−Boltzmann equation to obtain the double layer profile of counterions at each electrode, using as a boundary condition the instantaneous conducting ion concentration far from the electrode, effectively determining p, with μ then calculated from eq 4.

dx.doi.org/10.1021/cm103548t |Chem. Mater. 2011, 23, 1862–1873

The basic idea is that by using blocking electrodes the ions are allowed to polarize/accumulate near the electrodes at low frequency. The polarization of ions has two characteristics: (1) a significant increase of dielectric constant (ε') due to the increased effective capacitance resulting from storing counterions at the electrodes and (2) a decrease of ionic conductivity (σ') due to the compensation of voltage by polarized ions (Figure A-2a). Two important time scales can be defined to characterize EP:

$$\tau_\sigma \equiv \frac{\varepsilon_s \varepsilon_0}{\sigma_{DC}} \quad (5)$$

$$\tau_{EP} \equiv \frac{\varepsilon_{EP} \varepsilon_0}{\sigma_{DC}} \quad (6)$$

Here τ_σ is the time scale of conduction (where counterion mean-square displacement becomes diffusive) and τ_{EP} is the time scale for full electrode polarization. ε_s is the static (low frequency) dielectric constant of the sample, ε_{EP} is the dielectric constant when electrode polarization is complete and ε_0 is the vacuum permittivity. The Macdonald/Coelho model assumes that EP can be described by a simple Debye relaxation so the loss tangent peak can be fit to

$$\tan\delta = \frac{\varepsilon''}{\varepsilon'} = \frac{\omega\tau_{EP}}{1+\omega^2\tau_\sigma\tau_{EP}} \quad (7)$$

to obtain τ_σ and τ_{EP} (the peak frequency corresponds to the onset of electrode polarization, the geometric mean of τ_σ and τ_{EP}). Static dielectric constant can then be obtained from eq 5. By assuming that all anions are fixed on the polymer backbone and unable to move in the field, with no salt contaminants (single-ion conductors) the instantaneous conducting ion concentration and their mobility can be obtained:

$$\mu = \frac{eL^2\tau_\sigma}{4\tau_{EP}{}^2 kT} \quad (8)$$

$$p = \frac{\sigma_{DC}}{e\mu} = \frac{4\sigma_{DC}\tau_{EP}{}^2 kT}{e^2L^2\tau_\sigma} \quad (9)$$

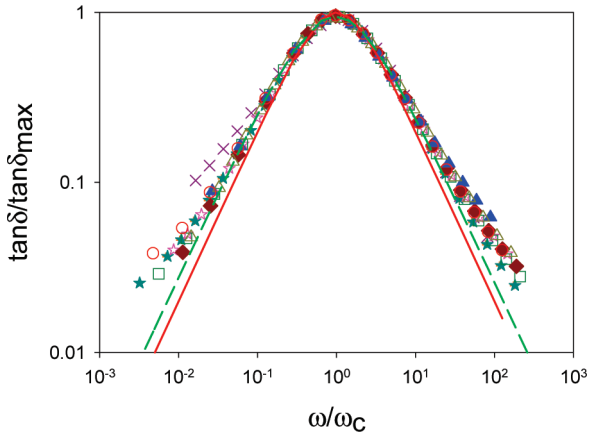

Figure 6. Fitted tanδ peak with eq 7 at T_g+20 K for different cations. X and Y axis are normalized with the peak value of tanδ and the geometric mean of τ_σ and τ_{EP}. Purple X is Na^+; orange plus is Me_4N^+; cyan solid star is $BuMeIm^+$; pink open star is $(MOE)MeIm^+$; green open square is $(EOc)_2Me(MOE)N^+$; dark red solid diamond is Bu_4N^+; blue solid triangle is Bu_4P^+; olive green open triangle is $Bu_3(MOE)P^+$; red open circle is $(MOEOE)_3MeN^+$; red solid line is best fitting for eq 7; green dashed line is best fitting for eq A-4.

where L is the sample thickness. Figure 6 displays the loss tangent data for different samples at T_g+20K fit to eq 7. All the samples have the same tanδ shape, indicating that the polarization process does not change with different cations. As observed previously for single-ion conductors[19,30,43] the loss tangent data are somewhat broader than the Debye relaxation of eq 7, but the fitting provides robust measures of τ_σ and τ_{EP}, from which mobility and conducting ion content are calculated using eqs 8 and 9, and ε_s is calculated using eq 5. Although the origins of the broader-than-Debye polarization are likely polymer/ion relaxation underneath EP, we fit EP to the broader Cole−Cole relaxation function[48,50,51] in the Appendix, resulting in better fits and similar τ_σ, τ_{EP}, p, and μ. Note that trapped counterions never participate in conduction and EP so they have no contribution to σ_{DC} and conducting ion content p, whereas all nontrapped counterions contribute to σ_{DC} beyond τ_σ. Among the nontrapped counterions, conducting ion content p are the ones participating ionic conductivity in an instantaneous snapshot and they exchange with other nontrapped counterions beyond τ_σ when conducting.

Equation 5 provides a method to determine static dielectric constant ε_S. In our system, the acid form precursor and Na^+ ionomer have ε_S = 14 near room temperature while all other ionomers have higher ε_S, which are between 20 to 30 (see Figure A-2b in the Appendix). Some counterions form ion pairs (which have strong dipoles) with the carboxylate and increase ε_S[43], whereas Na^+ has too strong Coulombic interaction and the majority of Na^+ are trapped in pPDI-carboxylate-pPDI segment, resulting in the same dielectric constant as the acid form precursor.

Concentrations of Conducting Ions and their Mobility. Conducting ion concentrations are plotted as a function of inverse temperature in Figure 7. The temperature dependence of conducting ion concentration calculated from eq 9 obeys an Arrhenius equation as shown in Figure 7

$$p = p_0 \exp\left(\frac{-E_a}{kT}\right) \quad (10)$$

where p_0 is the conducting ion concentration at infinite temperature and E_a is an activation energy; these parameters are

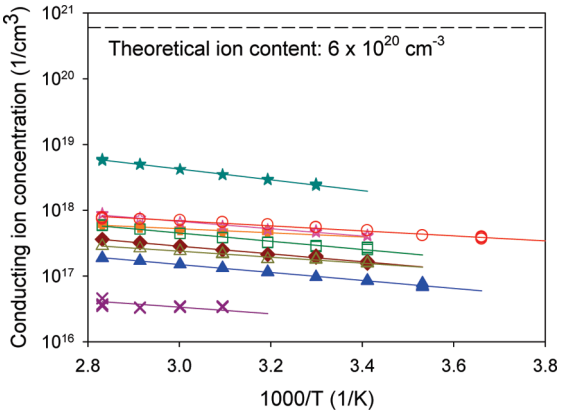

Figure 7. Conducting ion concentrations as functions of 1000/T. Purple X is Na^+; orange plus is Me_4N^+; cyan solid star is $BuMeIm^+$; pink open star is $(MOE)MeIm^+$; green open square is $(EOc)_2Me(MOE)N^+$; dark red solid diamond is Bu_4N^+; blue solid triangle is Bu_4P^+; olive green open triangle is $Bu_3(MOE)P^+$; red open circle is $(MOEOE)_3MeN^+$; solid lines are the best fits to the Arrhenius equation (eq 10).

shown in Table 3. Note that although the total ion concentration is about 6×10^{20} cm^{-3}, the "actual" amount of ions contributing to ionic conduction at any given time is much smaller and thermally activated, as reported previously.[19,30,43,52] The activation energy decreases with increasing cation size as expected, except for Na^+ and Me_4N^+. As discussed in the rheology section, our PU ionomers do not truly microphase separate but have local environments with different amount of pPDI-carboxylate-pPDI segments. The fact that p_0 is smaller than 6×10^{20} cm^{-3} indicates some of the counterions interact with these pPDI-carboxylate-pPDI segments too strongly to participate ionic conduction and the ratio $p_0/6 \times 10^{20}$ cm^{-3} tells us the fraction of counterions that are not trapped in these pPDI-carboxylate-pPDI rich local environments. The observation that Na^+ and Me_4N^+ samples have much lower p_0 and E_a suggest that the majority of ions are either trapped in pPDI-carboxylate-pPDI segments or aggregated, with few actually conducting.

In our system p_0, the amount of conducting counterions at infinite temperature, which we interpret to be the nontrapped ions participating in conduction at any temperature, is generally less than the total ion content 6×10^{20} cm^{-3} except the $BuMeIm^+$ ionomer. This is consistent with our previous discussion of morphology in the rheology section: most counterions except $BuMeIm^+$ are trapped in pPDI-carboxylate-pPDI segments.

Figure 8a plots mobility of the conducting ions against T_g/T, which is similar to the Figure 4 **inset** and Figure 5b **inset**. Like the α-relaxation frequency, the mobility has a VFT temperature dependence:

$$\mu = \mu_0 \exp\left(\frac{-DT_0}{T - T_0}\right) \tag{11}$$

and plotting against T_g/T merely reduces the data sets to a roughly one decade wide band. The solid curves in Figure 8 are fits of eq 11 with parameters summarized in Table 3. Unlike the α-relaxation frequency, Vogel temperature T_0 for mobility has a strong correlation with calorimetric T_g ($T_g - T_0 \approx 65$ K).

Figure 8b shows the correlation of α-relaxation frequency and conducting ion mobility, showing a slight decoupling (slope ~0.88−1.0). The origin of decoupling was generally considered as ion "hopping" transport under an electric field.[43,53] Figure 8b fails to collapse the data as well as Figure 5b. A simple interpretation stems from the fact that all ions that are not trapped in pPDI-carboxylate-pPDI segments participate in conduction beyond τ_σ and ω_α^{-1}. All non-trapped ions contribute equally to conduction. The average mobility is simply proportional to σ_{DC} and explains why the correlation between σ_{DC} and ω_α in Figure 5b works so well. In this scenario, the ionomer with sodium counterions simply has much more of Na^+ trapped, with about 1/6 fewer ions participating in conduction. In contrast, more of the larger counterions participate in conduction with much less or no counterions trapped. The apparent slope somewhat smaller than unity in Figure 8b then is simply caused by the Arrhenius temperature dependence of instantaneous conducting ion content in Figure 7.

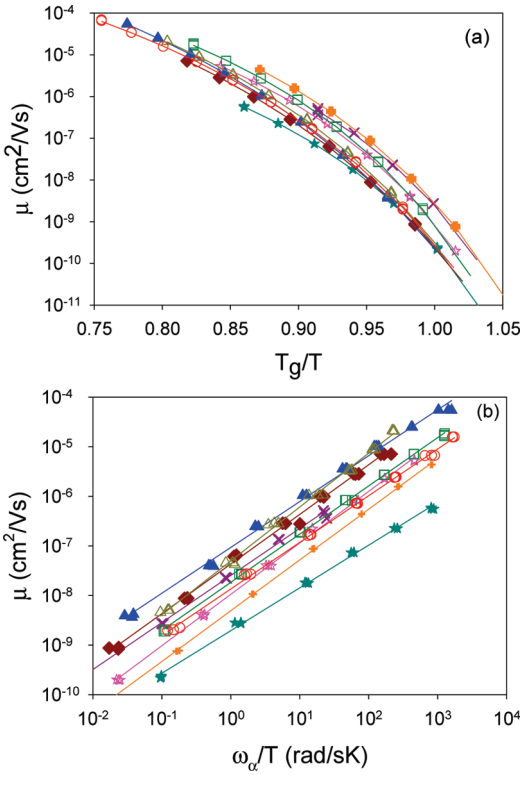

Figure 8. Cation mobility as function of (a) T_g/T (b) α relaxation frequency/temperature. Purple X is Na^+; orange plus is Me_4N^+; cyan solid star is $BuMeIm^+$; pink open star is $(MOE)MeIm^+$; green open square is $(EOc)_2Me(MOE)N^+$; dark red solid diamond is Bu_4N^+; blue solid triangle is Bu_4P^+; olive green open triangle is $Bu_3(MOE)P^+$; red open circle is $(MOEOE)_3MeN^+$; solid lines are the best fit power laws.

Actuation and Electrode Polarization (EP). The Macdonald/Coelho EP model allows us to obtain the electrode polarization time scale τ_{EP}, which is proportional to the electrode spacing L (sample film thickness).[30] A material property relevant for actuation, τ_{EP}/L can be obtained from eqs 5, 8 and 9:

$$\frac{\tau_{EP}}{L} = \frac{1}{\mu}\sqrt{\frac{\varepsilon_S \varepsilon_0}{4pkT}} \tag{12}$$

For fast actuation, ion-conducting membranes require small L and high conducting ion content p with high mobility μ.

Actuation can be modeled as an equivalent resistor-capacitor circuit, with the time scale for polarization (or charging) $\tau_{EP} = RC$, where R is the resistance and C is the capacitance of the equivalent circuit. The actuation is created on time scale τ_{EP} by a build-up of conducting ions in the Stern layer (within the Debye length of the electrode). The charge built up in the Stern layer Q can be described as a function of applied voltage: $Q = CV = \tau_{EP}V/R$, and the charge accumulation per unit electrode surface area A (charge density) can be calculated

$$\frac{Q}{A} = \frac{\tau_{EP}V}{RA} = \frac{\tau_{EP}V}{A}\frac{\sigma_{DC}A}{L} = \frac{\tau_{EP}}{L}V\sigma_{DC} \tag{13}$$

Hence, the charge density at the electrode is determined by the product of the material property τ_{EP}/L and conductivity σ_{DC}. Combining eqs 12 and 13, the charge density at the electrode can be rewritten as a function of conducting ion content p and static dielectric constant ε_S

$$\frac{Q}{A} = Ve\sqrt{\frac{\varepsilon_S \varepsilon_0 p}{4kT}} \tag{14}$$

Increase of conducting ion content and/or static dielectric constant can increase the charge density of polarizing ions and therefore increases the strain in the actuator. If we consider the strain of the actuator to be induced by the volume change as the

dx.doi.org/10.1021/cm103548t |Chem. Mater. 2011, 23, 1862–1873

result of counterion accumulation at the electrode, then a dimensionless parameter relevant to the strain can be estimated by multiplying polarizing charge density by cation volume V_{cation} divided by electrode spacing L

$$\frac{QV_{cation}}{AeL} \sim V_{cation}\varepsilon_S{}^{1/2}p^{1/2} \quad (15)$$

Figure 9a shows the volume of all polarized cations divided by membrane volume as a function of temperature with electrode spacing L of 100 μm. The Na-ionomers would make poor actuators because of the small size and lower conducting ion content of Na^+. Ionic liquid counterions should have strain 30−100× larger than Na^+. It is not surprising that the trend is similar to conducting ion content p in Figure 7 from its dependence on $p^{1/2}$. However, in Figure 9a $(MOEOE)_3MeN^+$ and $BuMeIm^+$ have similar highest value unlike in Figure 7, suggesting the importance of counterion size for generating strain.

Equations 13 and 14 also allow us to test the linear response assumption of the Macdonald/Coelho model. This model assumes that the build-up of ions near the electrode is sufficiently small that there is no interaction between ions polarized near the electrode. Nonlinear electrode polarization will occur when polarizing ions start to interact with each other — when they are separated by the Bjerrum length on the electrode surface (where their Coulomb repulsion equals to thermal energy).

$$l_B = \frac{e^2}{4\pi\varepsilon_0\varepsilon_S kT} \quad (16)$$

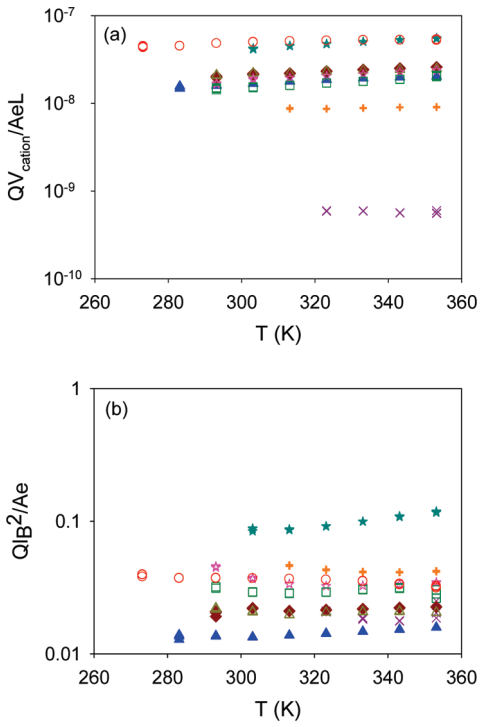

Figure 9. (a) Dimensionless strain relevant parameter (eq 15) as a function of temperature with electrode spacing of 100 μm and assuming cations have density of 1 g/cm^3. (b) Dimensionless charge density parameter (Eq18) as a function of temperature. The fact that $Ql_B{}^2/Ae < 1$ suggests linear EP response. Purple X is Na^+; orange plus is Me_4N^+; cyan solid star is $BuMeIm^+$; pink open star is $(MOE)MeIm^+$; green open square is $(EOc)_2Me(MOE)N^+$; dark red solid diamond is Bu_4N^+; blue solid triangle is Bu_4P^+; olive green open triangle is $Bu_3(MOE)P^+$; red open circle is $(MOEOE)_3MeN^+$.

The relevant dimensionless parameter, $Ql_B{}^2/(Ae)$ the ions polarized per squared Bjerrum length, should be smaller than unity to ignore nonlinear effects and unilize the Macdonald/Coelho model to estimate conducting ion content

$$\frac{Ql_B{}^2}{Ae} = \frac{\tau_{EP}V\sigma_{DC}l_B{}^2}{Le} = \frac{\tau_{EP}eV\sigma_{DC}l_B}{4\pi\varepsilon_0\varepsilon_S kTL} < 1 \quad (17)$$

or

$$\frac{Ql_B{}^2}{Ae} = Vl_B{}^2\sqrt{\frac{\varepsilon_S\varepsilon_0 p}{4kT}} = \frac{eV}{kT}\sqrt{\frac{pl_B{}^3}{16\pi}} < 1 \quad (18)$$

Figure 9b shows this dimensionless parameter as a function of temperature. For all ionomers studied in this paper, $Ql_B{}^2/Ae$ is in the range of 0.1 to 0.01, which is well below 1. This verifies that our ionomer system is in the linear region with 0.1 V applied, through the temperature range we study and justifies the linear assumption of the Macdonald/Coelho EP model we use to separate the conductivity into instantaneous conducting ion content p and their mobility μ. Figure 9a also shows why real actuators require added ions, larger voltages and thinner films in the strongly nonlinear EP range for actuation, as the strains of order 1×10^{-8} at 0.1 V will not be observable.

CONCLUSION

Influence of various cationic counterions on both thermal and dielectric properties of PEO-based polyurethane carboxylate ionomers has been studied. Size and species of cations play important roles. Generally, larger cations result in lower T_g because of weaker Coulombic attraction with anions.

Ionic conductivity in these single-ion conductors is strongly correlated with α-relaxation frequency of PEO. This implies ion conduction is strongly coupled with polymer segmental relaxation, as expected for ionomers with strong solvation interaction between the polymer and counterions. Electrode polarization at low frequencies is used to determine conducting ion concentration and mobility. Conducting ion mobility shows VFT behavior with strong correlations to both polymer chain relaxation and T_g, while the conducting ion concentration has an Arrhenius temperature dependence. We found that significant amounts of counterions are trapped by pPDI-carboxylate-pPDI segments, with only small portions contributing to ionic conductivity. From the observed Arrhenius temperature dependence of instantaneous conducting ion content, about 90% of the counterions are trapped in pPDI-carboxylate-pPDI segment for most of the ionomers except $BuMeIm^+$, which has almost no trapped counterions and Na^+, which has more than 98% trapped. At any instantaneous snapshot, the Na^+ sample has fewer than 0.01% conducting ions. Me_4N^+ has about 0.1% conducting and all other larger cations have 0.1−1% of the cations conducting. Unfortunately, while pPDI strongly microphase separates in neutral polyurethane,[21] interaction with ions and PEO prevents discrete microphase separation in pPDI-PEO-ionomers. Consequently the modulus is too low for these materials to be useful as ionic actuators.

We have proven that larger counterions lower T_g and boost ion conductivity, with our custom-synthesized ammonium with three ethylene oxide tails having by far the highest ionic conductivity. That counterion shows great promise for ionic actuators, which need large counterions for large strain and high ionic conductivity for fast response. To further improve conductivity, large phosphonium cations with a suitable amount of

ether oxygen atoms attached in a high dielectric constant ion-solvating polymer matrix is the direction to increase both conducting ion concentration and cation mobility.

APPENDIX

Broader spectra than Debye prediction (Figure 6) are commonly observed for electrode polarization of ionomers.[30,43,50,51] Cole and Cole introduced a parameter α to the Debye equation to allow a description of broadened relaxations that maintain symmetry on a log frequency scale,[51]

$$\varepsilon_{EP}^{*} = \varepsilon_s + \frac{\varepsilon_{EP} - \varepsilon_s}{1 + (i\omega\tau_0)^{1-\alpha}} \quad \text{(A-1)}$$

where $0 \le \alpha \le 1$. It is identical to the Debye equation when $\alpha = 0$. So ε', ε'' and loss tangent tan δ can be derived[16,51]

$$\varepsilon_{EP}' = \varepsilon_s + \frac{(\varepsilon_{EP} - \varepsilon_s)\left[1 + (\omega\tau_0)^{1-\alpha}\sin(\tfrac{1}{2}\alpha\pi)\right]}{1 + 2(\omega\tau_0)^{1-\alpha}\sin(\tfrac{1}{2}\alpha\pi) + (\omega\tau_0)^{2(1-\alpha)}} \quad \text{(A-2)}$$

$$\varepsilon_{EP}'' = \frac{(\varepsilon_{EP} - \varepsilon_s)(\omega\tau_0)^{1-\alpha}\cos(\tfrac{1}{2}\alpha\pi)}{1 + 2(\omega\tau_0)^{1-\alpha}\sin(\tfrac{1}{2}\alpha\pi) + (\omega\tau_0)^{2(1-\alpha)}} \quad \text{(A-3)}$$

$$\tan\delta = \frac{\varepsilon_{EP}''}{\varepsilon_{EP}'} = \left[\frac{1}{(\omega\tau_0)^{1-\alpha}\cos(\tfrac{1}{2}\alpha\pi)} + \tan(\frac{1}{2}\alpha\pi) + \frac{\tau_\sigma}{\tau_{EP}}\frac{(\omega\tau_0)^{1-\alpha}}{\cos(\tfrac{1}{2}\alpha\pi)}\right]^{-1} \quad \text{(A-4)}$$

by the assumption $\varepsilon_{EP} \gg \varepsilon_s$.[30] The fitting is shown in Figure 6 (green dashed line). Note that τ_0 here is not the relaxation time in eq 7. Time scales of conduction τ_σ and electrode polarization τ_{EP} can be obtained by the fact that the maximum in tanδ is at the geometric mean of τ_σ and τ_{EP}. Equation A-5 gives the relationship between τ_0, τ_σ and τ_{EP}:

$$\tau_0 = \tau_\sigma^{\alpha/2(\alpha-1)}\tau_{EP}^{(\alpha-2)/2(\alpha-1)} \quad \text{(A-5)}$$

Figure A-1 shows the comparison of τ_σ and τ_{EP} obtained by eq 7 and eq A-5. It is interesting how well they agree with each other

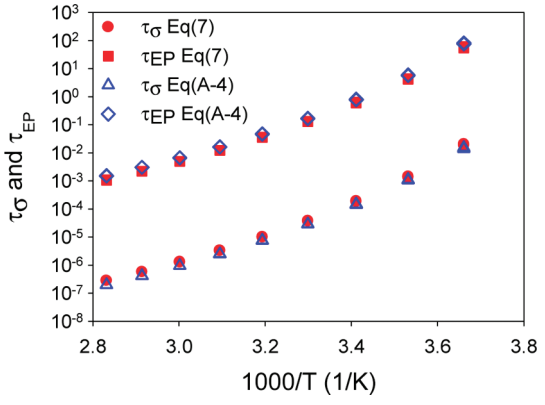

Figure A-1. Comparison of τ_σ and τ_{EP} obtained from eq 7 (solid symbols) and eq A-4 (open symbols) with $\alpha = 0.007$.

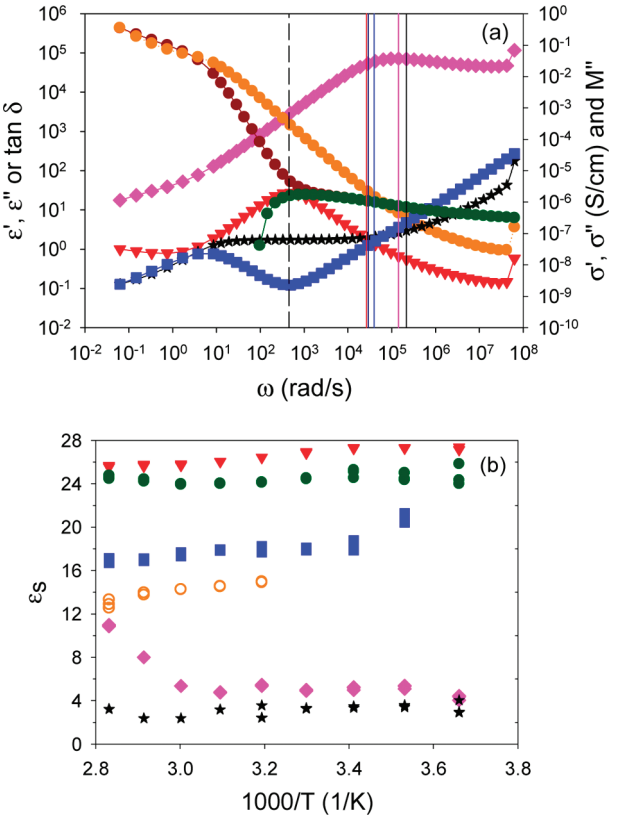

Figure A-2. (a) Dielectric spectra for $(MOEOE)_3MeN^+$ at 30 °C. Left y axis: dark red circle is ε''; orange circle is ε''; red triangle is tan δ; green circle is $\varepsilon'$with EP subtracted as a power law. Right y axis: black star is σ'; blue square is σ''; pink diamond is M''. In the order of increasing frequency, the dashed line is the geometric mean of τ_σ and τ_{EP}; red line is $\tau_{\sigma,\tan\delta}$; green line is $\tau_{\sigma,\varepsilon'}$; blue line is $\tau_{\sigma,\sigma''}$; pink line is $\tau_{\sigma,M''}$; black line is $\tau_{\sigma,\sigma'}$. (b) Comparison of ε_s obtained by different method: red triangle is $\varepsilon_{s,\tan\delta}$; green circle is $\varepsilon_{s,\varepsilon'}$; blue square is $\varepsilon_{s,\sigma''}$; pink diamond is $\varepsilon_{s,M''}$, black star is $\varepsilon_{s,\sigma'}$; orange open circle is ε_s for the acid form for reference.

because the EP relaxations are only slightly broader than Debye, but τ_{EP} increases slightly and τ_σ decreases slightly with the broader Cole−Cole spectrum, as expected. For simplicity, τ_σ and τ_{EP} discussed in this paper are obtained by eq 7. Note that time−temperature-superposition does not apply to EP and the ratio τ_{EP}/τ_σ increases with temperature, due to the fact that conducting ion content weakly increases with temperature.

Static dielectric constant ε_s is generally defined as the high frequency plateau of $\varepsilon'(\omega)$ spectra before electrode polarization begins, as shown in Figure A-2a. However, the exact value of the $\varepsilon'(\omega)$ plateau is rather difficult to be identified in ionomers because of the nonflat nature of $\varepsilon'(\omega)$ just before EP, indicating underlying relaxations. Several ways to determine ε_s are summarized in Table A-1 and the corresponding time scale and ε_s are shown in panels a and b in Figure A-2. Note that the time scales of ion conduction (τ_σ, eq 5) and EP (τ_{EP}, eq 6) are correlated by the fact that the peak frequency of tan δ is the geometric mean of these two time scales

$$\tau_{\tan\delta,\max} = \sqrt{\tau_\sigma\tau_{EP}} \quad \text{(A-6)}$$

Among the various measures of diffusive motion of counterions (see Table A-1), $\tau_{\sigma,\tan\delta} \sim \tau_{\sigma,\varepsilon'} > \tau_{\sigma,\sigma''} > \tau_{\sigma,M''} > \tau_{\sigma,\sigma'}$ and $\varepsilon_{s,\tan\delta} \sim \varepsilon_{s,\varepsilon'} >$

dx.doi.org/10.1021/cm103548t |Chem. Mater. 2011, 23, 1862–1873

Table A-1. Summary of different methods to obtain conduction time scale and static dielectric constants

conduction time scale	static dielectric constant	physical meaning of the time scale	method	ref
$\tau_{\sigma,\tan\delta}$	$\varepsilon_{S,\tan\delta}$	diffusive conduction	eqs 5 and 7	30
$\tau_{\sigma,\varepsilon'}$	$\varepsilon_{\sigma,\varepsilon'}$	diffusive conduction	directly obtained from the plateau region of $\varepsilon'-\omega^n$	
$\tau_{\sigma,\sigma''}$	$\varepsilon_{\sigma,\sigma''}$	EP completed at $\sigma''_{min} = \sigma''(\tau_{EP})$	$\sigma''_{min} = \sigma''(\tau_{EP})$ and eq A-6	54
$\tau_{\sigma,M''}$	$\varepsilon_{\sigma,M''}$	hopping conduction	$M''_{max} = M''(\tau_{\sigma,M''})$	54
$\tau_{\sigma,\sigma'}$	$\varepsilon_{\sigma,\sigma'}$	hopping conduction	$\sigma'(\tau_{\sigma,\sigma'}) = 2\sigma_{DC}$	55

$\varepsilon_{s,\sigma''} > \varepsilon_{s,M''} > \varepsilon_{s,\sigma'}$. τ_σ and ε_s calculated from M'' and σ'' have much smaller value than other methods and are less suitable in our system. Notice that $\varepsilon_{s,M''}$ and $\varepsilon_{s,\sigma''}$ are even smaller than the dielectric constant of the acid form of our polyurethane which is less likely because the ionomer form has much stronger dipole than the acid form (1.77 D) from ab initio calculations. For discussions in this paper, we adopt the static dielectric constant from fitting tan δ to the Debye function (eq 7) because it has good agreement with the ε_s obtained from the plateau value before EP begins by subtracting the EP contribution ($\sim \omega^n$) from $\varepsilon'(\omega)$, and is more robust.

AUTHOR INFORMATION

Corresponding Author

*E-mail: rhc@plmsc.psu.edu.

ACKNOWLEDGMENT

This material is based on work supported in part by the U.S. Army Research Office under Grant W911NF-07-1-0452 Ionic Liquids in Electro-Active Devices (ILEAD) MURI. We thank Michael Janik, Timothy Long, Sean Ramirez, James Runt, and Qiming Zhang for helpful discussions; Matthew Green for molecular weight determination; and Wenqin Wang and Karen Winey for X-ray scattering. S.-W.W. also thanks Air Products and Chemicals, Inc., for a fellowship that exposed her to polyurethane synthesis in the summer of 2008.

REFERENCES

(1) Fenton, D. E.; Parker, J. M.; Wright, P. V. *Polymer* **1973**, *14*, 589.
(2) Meyer, W. H. *Adv. Mater.* **1998**, *10*, 439–448.
(3) Gadjourova, Z.; Andreev, Y. G.; Tunstall, D. P.; Bruce, P. G. *Nature* **2001**, *412*, 520–523.
(4) Snyder, J. F.; Carter, R. H.; Wetzel, E. D. *Chem. Mater.* **2007**, *19*, 3793–3801.
(5) Singh, M.; Odusanya, O.; Wilmes, G. M.; Eitouni, H. B.; Gomez, E. D.; Patel, A. J.; Chen, V. L.; Park, M. J.; Fragouli, P.; Iatrou, H.; Hadjichristidis, N.; Cookson, D.; Balsara, N. P. *Macromolecules* **2007**, *40*, 4578–4585.
(6) Gomez, E. D.; Panday, A.; Feng, E. H.; Chen, V.; Stone, G. M.; Minor, A. M.; Kisielowski, C.; Downing, K. H.; Borodin, O.; Smith, G. D.; Balsara, N. P. *Nano Lett.* **2009**, *9*, 1212–1216.
(7) Ramesh, S.; Radhakrishnan, G. *J. Polym. Mater.* **1999**, *16*, 135–153.
(8) Ding, Y. S.; Register, R. A.; Yang, C.-z.; Cooper, S. L. *Polymer* **1989**, *30*, 1204–1212.
(9) Visser, S. A.; Cooper, S. L. *Macromolecules* **1991**, *24*, 2576–2583.
(10) Williams, S. R.; Wang, W.; Winey, K. I.; Long, T. E. *Macromolecules* **2008**, *41*, 9072–9079.
(11) Yang, C.-Z.; Grasel, T. G.; Bell, J. L.; Register, R. A.; Cooper, S. L. *J. Polym. Sci., Part B: Polym. Phys.* **1991**, *29*, 581–588.
(12) Chen, S.-A.; Hsu, J.-S. *Polymer* **1993**, *34*, 2769–2775.
(13) Lee, D.-c.; Register, R. A.; Yang, C.-z.; Cooper, S. L. *Macromolecules* **1988**, *21*, 1005–1008.
(14) Xu, H.-S.; Yang, C.-Z. *J. Polym. Sci., Part B: Polym. Phys.* **1995**, *33*, 745–751.
(15) Jayakumar, R.; Nanjundan, S.; Prabaharan, M. *J. Macromol. Sci., Part C: Polym. Rev.* **2005**, *45*, 231–261.
(16) Kremer, F.; Schonhals, A. *Broadband Dielectric Spectroscopy*; Springer: New York, 2003.
(17) Pissis, P.; Polizos, G. In *Handbook of Condensation Thermoplastic Elastomers*; Fakirov, S., Ed.; Wiley-VCH: Weinheim, Germany, 2005, pp 381−434.
(18) Polizos, G.; Georgoussis, G.; Kyritsis, A.; Shilov, V. V.; Shevchenko, V. V.; Gomza, Y. P.; Nesin, S. D.; Klimenko, N. S.; Wartewig, S.; Pissis, P. *Polym. Int.* **2000**, *49*, 987–992.
(19) Fragiadakis, D.; Dou, S.; Colby, R. H.; Runt, J. *Macromolecules* **2008**, *41*, 5723–5728.
(20) Wei, X.; Yu, X. *J. Polym. Sci., Part B: Polym. Phys.* **1997**, *35*, 225–232.
(21) Sheth, J. P.; Klinedinst, D. B.; Wilkes, G. L.; Yilgor, I.; Yilgor, E. *Polymer* **2005**, *46*, 7317–7322.
(22) Ishida, M.; Yoshinaga, K.; Horii, F. *Macromolecules* **1996**, *29*, 8824–8829.
(23) Becke, A. D. *J. Chem. Phys.* **1993**, *98*, 5648–5652.
(24) Lee, C. T.; Yang, W. T.; Parr, R. G. *Phys. Rev. B* **1988**, *37*, 785–789.
(25) Vosko, S. H.; Wilk, L.; Nusair, M. *Can. J. Phys.* **1980**, *58*, 1200–1211.
(26) Stephens, P. J.; Devlin, F. J.; Chabalowski, C. F.; Frisch, M. J. *J. Phys. Chem.* **1994**, *98*, 11623–11627.
(27) Liu, W. Doctoral Dissertation, The Pennsylvania State University, State College, PA, 2011.
(28) Al-Salah, H. A.; Frisch, K. C.; Xiao, H. X.; McLean, J. A., Jr. *J. Polym. Sci., Part A: Polym. Chem.* **1987**, *25*, 2127–2137.
(29) Chen, H.; Chen, D.; Fan, Q.; Yu, X. *J. Appl. Polym. Sci.* **2000**, *76*, 2049–2056.
(30) Klein, R. J.; Zhang, S.; Dou, S.; Jones, B. H.; Colby, R. H.; Runt, J. *J. Chem. Phys.* **2006**, *124*, 144903.
(31) Eisenberg, A. *Macromolecules* **1971**, *4*, 125–128.
(32) Weiss, R. A.; Agarwal, P. K.; Lundberg, R. D. *J. Appl. Polym. Sci.* **1984**, *29*, 2719–2734.
(33) Eisenberg, A.; Kim, J.-S. *Introduction to Ionomers*; Wiley-Interscience: New York, 1998.
(34) Pauling, L. *The Nature of the Chemical Bond and the Structure of Molecules and Crystals: An Introduction to Modern Structural Chemistry*, 3rd ed.; Cornell University Press: Ithaca, NY, 1960.
(35) Weiss, R. A.; Agarwal, P. K. *J. Appl. Polym. Sci.* **1981**, *26*, 449–462.
(36) Weiss, R. A.; Stamato, H. *Polym. Eng. Sci.* **1989**, *29*, 134–139.
(37) Velankar, S.; Cooper, S. L. *Macromolecules* **1998**, *31*, 9181–9192.
(38) Velankar, S.; Cooper, S. L. *Macromolecules* **2000**, *33*, 395–403.
(39) Han, C. D. In *Rheology and Processing of Polymeric Materials*; Oxford University Press: New York, 2007; Vol. 1, pp 484−486.
(40) Lu, X.; Weiss, R. A. *Macromolecules* **1995**, *28*, 3022–3029.
(41) Smith, G. D.; Borodin, O.; Li, L. Y.; Kim, H.; Liu, Q.; Bara, J. E.; Gin, D. L.; Nobel, R. *Phys. Chem. Chem. Phys.* **2008**, *10*, 6301–6312.
(42) Huang, K.; Han, X.; Zhang, X.; Armstrong, D. W. *Anal. Bioanal. Chem.* **2007**, *389*, 2265–2275.
(43) Fragiadakis, D.; Dou, S.; Colby, R. H.; Runt, J. *J. Chem. Phys.* **2009**, *130*, 064907.

(44) Wubbenhorst, M.; van Turnhout, J. *J. Non-Cryst. Solids* **2002**, *305*, 40–49.
(45) Zhang, S.; Dou, S.; Colby, R. H.; Runt, J. *J. Non-Cryst. Solids* **2005**, *351*, 2825–2830.
(46) Angell, C. A. *Proc. Natl. Acad. Sci. U.S.A.* **1995**, *92*, 6675–6682.
(47) Borodin, O.; Smith, G. D. *Macromolecules* **2006**, *39*, 1620–1629.
(48) Macdonald, J. R. *Phys. Rev.* **1953**, *92*, 4–17.
(49) Coelho, R. *J. Non-Cryst. Solids* **1991**, *131−133*, 1136–1139.
(50) Macdonald, J. R. *J. Chem. Phys.* **1974**, *61*, 3977–3996.
(51) Cole, K. S.; Cole, R. H. *J. Chem. Phys.* **1941**, *9*, 341–351.
(52) Ratner, M. A.; Shriver, D. F. *Chem. Rev.* **1988**, *88*, 109–124.
(53) Ratner, M. A.; Nitzan, A. *Faraday Discuss. Chem. Soc.* **1989**, *88*, 19–42.
(54) Sangoro, J. R.; Serghei, A.; Naumov, S.; Galvosas, P.; Karger, J.; Wespe, C.; Bordusa, F.; Kremer, F. *Phys. Rev. E* **2008**, *77*, 051202.
(55) Dyre, J. C.; Maass, P.; Roling, B.; Sidebottom, D. L. *Rep. Prog. Phys.* **2009**, *72*, 046501.